Offset energies at organic semiconductor heterojunctions and their influence on the open-circuit voltage of thin-film solar cells

Barry P. Rand and Diana P. Burk
Department of Electrical Engineering and Princeton Institute for the Science and Technology of Materials (PRISM), Princeton University, Princeton, New Jersey 08544, USA

Stephen R. Forrest*
Departments of Electrical Engineering and Computer Science, Physics, and Materials Science and Engineering, University of Michigan, Ann Arbor, Michigan 48109, USA

(Received 2 October 2006; revised manuscript received 17 January 2007; published 27 March 2007)

Organic semiconductor heterojunction (HJ) energy level offsets are modeled using a combination of Marcus theory for electron transfer, and generalized Shockley theory of the dark current density vs voltage (*J-V*) characteristics. This model is used to fit the *J-V* characteristics of several donor-acceptor combinations commonly used in thin film organic photovoltaic cells. In combination with measurements of the energetics of donor-acceptor junctions, the model predicts tradeoffs between the junction open-circuit voltage (V_{OC}) and short-circuit current density (J_{SC}). The V_{OC} is found to increase with light intensity and inversely with temperature for 14 donor-acceptor HJ materials pairs. In particular, we find that V_{OC} reaches a maximum at low temperature ($\sim$175 K) for many of the heterojunctions studied. The maximum value of V_{OC} is a function of the difference between the donor ionization potential and acceptor electron affinity, minus the binding energy of the dissociated, geminate electron-hole pair: a general relationship that has implications on the charge transfer mechanism at organic heterojunctions. The fundamental understanding provided by this model leads us to infer that the maximum power conversion efficiency of double heterostructure organic photovoltaic cells can be as high as 12%. When combined with mixed layers to increase photocurrent and stacked cells to increase V_{OC}, efficiencies approaching 16% are within reach.

DOI: 10.1103/PhysRevB.75.115327 PACS number(s): 73.40.Lq, 72.80.Le, 71.35.−y

I. INTRODUCTION

Semiconductor heterojunctions (HJ) are an ubiquitous feature of almost all photonic device structures, as they are useful in locally confining or controlling both charge and photons.[1] One of the most important issues facing the study of heterojunctions in new materials systems is the magnitude and the origin of the heterobarrier between dissimilar, contacting semiconductors. In contrast to inorganic heterojunctions, organic HJs generally do not have a significant amount of free charge that redistribute when materials are brought into contact.[2] Furthermore, their energetics are rarely influenced by the crystalline morphology at the interface since most of these van der Waals bonded materials do not require lattice matching to form ordered structures.[3] Both of these factors lead to a considerable simplification in our ability to quantitatively determine the source of the heterobarrier, and to grow organic heterojunctions to test these theories over an exceptionally wide range of materials properties. Hence, they present an opportunity to understand many of the factors governing the nature of charge transport and energetics of this most fundamental semiconductor property.

Among the class of organic HJs that are important to investigate, donor-acceptor (*DA*) junctions used in organic photovoltaic (PV) cells are key to cell efficiency, as they are the site for photogenerated exciton dissociation and charge transfer into the contacting materials forming this active junction. For this reason, the PV cell represents an ideal vehicle for studying HJ properties. Indeed, organic PV cells based on small-molecular weight materials and conjugated polymers have recently attracted interest as a potential approach to realizing low cost solar energy conversion.[4–6] Despite gains in power conversion efficiency (η_P) to approximately 5% for both small-molecule and polymer-based structures,[7,8] further improvements are necessary to realize practical devices. To fully optimize these PV cells, there needs to be a more complete understanding of the physics governing their operation, and in particular, the physics of photoinduced charge transfer at the *DA* HJ.

One issue of considerable focus in *DA* HJs has been the HJ open-circuit voltage (V_{OC}), typically in the range of 0.5 V to 1 V,[9] whereas the peak absorption of the solar spectrum of the constituent organic materials is at photon energies $>$2.5 eV. In principle, if qV_{OC} (where q is the electron charge) approaches the photon energy, organic solar cells would be 2 to 5 times more efficient than currently obtained. The experimental effort to determine the origin of the low V_{OC} has primarily consisted of understanding observed correlations between V_{OC} and the difference between the highest occupied molecular orbital (HOMO) of the donor material and lowest unoccupied molecular orbital (LUMO) of the acceptor.[9–14] This correlation is consistent with the fact that V_{OC} is a property of the *DA* energy levels and their offsets at the contacting heterointerface rather than due to the work function differences between the metal electrodes, as has also been proposed.[10]

To understand the fundamental physics governing V_{OC} and its relationship with the offset energies at *DA* HJs, in this work we measure the *maximum* V_{OC} attainable in organic PV cells based on a variety of combinations of donor and accep-

tor materials. To determine this maximum value, either temperature is reduced or light intensity increased until V_{OC} reaches saturation. The maximum value of V_{OC} is found to be related to the donor HOMO and acceptor LUMO energies, as well as the binding energy of the dissociated, geminate electron-hole pair created as a result of electron transfer.

To explore the dependence of V_{OC} on the energetic properties of the contacting materials, we present a comprehensive model for organic *DA* HJs based on molecular materials commonly employed in PV cells. The dark currents of various HJs are modeled using a generalized Shockley equation for *p-n* junctions.[15] By adapting a model for electron transfer based on nonadiabatic Marcus theory[16] to determine the photocurrent as a function of voltage, we fit the response of different *DA* HJ PV cells as functions of temperature and illumination intensity to extract the electron transfer rates. These rates are shown to follow the predictions of Marcus theory of electron transfer,[17] including an inverted region at a large *DA* offset energy. Applying this theory reveals that η_P approaching 12% is feasible for a single *DA* HJ, and possibly up to 16% by incorporating other more complex architectures,[7,18,19] demonstrating that practical efficiencies are within reach.

This paper is organized as follows: In Sec. II, we describe the principles of photocurrent generation at a *DA* HJ. This includes a presentation of quantitative models for the photocurrent and dark current, and the maximum, or saturated value of V_{OC} based on Marcus theory as applied to a heterointerface in combination with Shockley's theory for *p-n* junctions. Experimental details are described in Sec. III. The dependence of the dark current and PV operating parameters on temperature and HJ composition are provided in Sec. IV. Section V presents a discussion of the key findings as well as model predictions for the maximum η_P in *DA* HJ solar cells consisting of materials and structures analogous to those studied here. We provide conclusions in Sec. VI. A detailed derivation of the current model is given in the Appendix.

II. THEORY

A. Photocurrent at a donor-acceptor heterojunction

A schematic energy diagram for an organic HJ based on a contact between a donor and acceptor material is shown in Fig. 1. The difference between the ionization potential (IP) and electron affinity (EA) is known as the transport gap, E_{tran}. The optical energy gap of each material, E_{opt}, is defined as the position of the low-energy absorption edge. The exciton binding energy is E_B=IP−EA−E_{opt}, which typically ranges from 0.2 eV to 1 eV for organic semiconductors.[20,21]

The external quantum efficiency, η_{EQE}, determines the number of electrons collected per incident photon. For the organic HJ, η_{EQE} is[22]

$$\eta_{EQE}(\lambda, V) = \eta_A(\lambda)\,\eta_{ED}\,\eta_{CT}(V)\,\eta_{CC}(V). \quad (1)$$

Here, η_A is the absorption efficiency of the incident photons in the photoactive region resulting in the formation of excitons, η_{ED} is the efficiency of photogenerated excitons that diffuse to the *DA* interface, η_{CT} is the charge transfer efficiency for excitons to dissociate into holes in the donor and electrons in the acceptor layers at the HJ, and η_{CC} is the charge collection efficiency, equal to the fraction of photogenerated charge carriers collected at the electrodes. The wavelength of the incident light is λ, and V is the applied voltage.

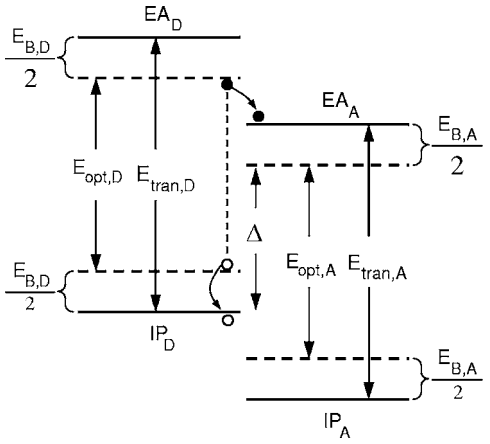

FIG. 1. Proposed energy level diagram of an organic heterojunction between a donor (D) and an acceptor (A) layer. Here IP and EA are the ionization potential and electron affinity, respectively. The exciton binding energy (E_B) of each material is equal to the difference between the transport gap (E_t) and optical gap (E_{opt}). Also, Δ is the interface energy gap. The process of charge transfer of an exciton from $D \rightarrow A$ is also illustrated.

To determine η_A, the dielectric constants, thicknesses, and optical field intensities within the active layers are required. The exciton diffusion length, L_D, determines η_{ED}, where L_D is from 5 nm to 30 nm for most photoactive molecular organic materials used in PV cells.[22] When the energy level offsets for the HOMO or LUMO between the donor and acceptor layers (ΔE_{HOMO} or ΔE_{LUMO}, respectively) are greater than E_B, charge transfer at the *DA* interface is energetically favorable, as shown in Fig. 1.

Both η_{CT} and η_{CC} are functions of V, as implied by Eq. (1). To evaluate these efficiencies, we adapt nonadiabatic Marcus theory to molecular organic HJs, as described by Nelson *et al.*[16] A representation of the model is shown in Fig. 2, where unshaded arrows correspond to the contribution to the donor photocurrent (J_D), while shaded arrows represent contributions to the acceptor photocurrent (J_A). The excited electron may be transferred from the donor LUMO, E_{cD} to the acceptor LUMO, E_{cA}. Similarly, the hole is transferred from the acceptor HOMO, E_{vA} to the donor HOMO, E_{vD}. The quasi-Fermi levels, μ (dotted lines in Fig. 2), determine the occupation probabilities of the various energy levels at voltage, V, (i.e., $f_i=\{1+\exp[(E_i-\mu_i)/k_BT]\}^{-1}$, where f is the occupation probability, k_B is Boltzmann's constant, and T is the temperature). Here, we outline the steps used to calculate J_D, where the calculation of J_A follows an analogous procedure.

The method for calculating the current density generated by light absorption, G_{vcD}, is provided in the Appendix [cf. Eq. (A1)]. Here, the first two lower-case subscripts refer to a transition from the valence level, v, or HOMO, to the conduction level, c, or LUMO. The third subscript corresponds to either donor, D, or acceptor, A, as in Fig. 2. Thus, G_{vcD} is

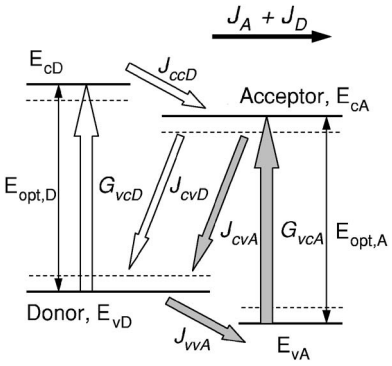

FIG. 2. Schematic of the various contributions to the current generated at a donor-acceptor heterojunction. Unshaded arrows correspond to the donor photocurrent while shaded arrows represent contributions to the acceptor photocurrent. Dotted lines show the Fermi energy levels. The subscripts v, c, A, and D refer to the valance and conduction energy levels in the acceptor and donor layers, respectively. For example, J_{cvD} is the current from the conduction level of the acceptor flowing to the valance level of the donor. Also, opt refers to energy gaps measured by optical means.

the source current for electron transfer, from which the efficiencies, η_{CT} and η_{CC}, are calculated. The forward and reverse current densities, J_{ccD} and J_{cvD}, respectively, are calculated using[16]

$$J_{if} = qk_{if}[f_i(1-f_f) - \exp(-E_{if}/k_BT)f_f(1-f_i)]. \quad (2)$$

Here, i and f represent initial and final energy levels that correspond to the first two subscripts of the currents given in Fig. 2. The Boltzmann factor is due to the junction energy barrier to reverse current flow. The free energy difference between i and f is $E_{if}=E_i-E_f$, and k_{if} is the electron transfer rate, given by nonadiabatic Marcus theory[17] as

$$k_{if} = \left(\frac{4\pi^3}{h^2\lambda_{if}k_BT}\right)^{1/2} V_{if}^2 \exp\left(-\frac{(E_{if}+\lambda_{if})^2}{4\lambda_{if}k_BT}\right). \quad (3)$$

Here, V_{if} is the electronic coupling matrix element, assumed to be equal for a given DA pair, h is Planck's constant, and λ_{if} is the molecular reorganization energy. In the case of forward electron transfer (k_{ccD}), E_B is added to E_{if}, thereby reducing the electron transfer rate (for exothermic transfer, $E_{if}<0$).

To determine $\eta_{CT}(V)$ and $\eta_{CC}(V)$, J_D is calculated as a function of the difference in quasi-Fermi energies in the D and A materials. The Fermi level is $\mu_0=E_v+E_{tran}/2$ at equilibrium. Then, $J_D=J_{ccD}-J_{cvD}$ and $G_{vcD}=J_{ccD}+J_{cvD}$, while $qV=\mu_a-\mu_d=2(\mu_a-\mu_0)$, where μ_a (μ_d) is the quasi-Fermi level of the acceptor (donor) layer. A solution is found using a set of parametric equations (see Appendix) to calculate the possible occupation probabilities (and therefore V). From the resulting J_D-V characteristic, we calculate the collection function, $H(V)$, for the donor photocurrent contribution, *viz.*,

$$H_D(V) = \eta_{CT}(V)\,\eta_{CC}(V) = \left(\frac{k_{ccD}}{k_{ccD}+k_{cvD}}\right)\frac{J_D}{q\phi_s}, \quad (4)$$

where ϕ_s is the optical absorption rate (see Appendix), and the total $H(V)=H_D(V)+H_A(V)$.

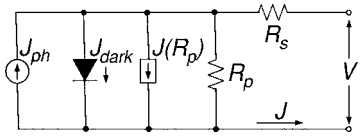

FIG. 3. Equivalent circuit for an organic heterojunction used to understand the current density versus voltage (J-V) model. The specific series and parallel resistances are R_s and R_p, respectively, $J(R_p)$ is the current density due to R_p, and J_{dark} and J_{ph} the dark and photocurrent densities, respectively.

B. Current-voltage characteristics of the donor-acceptor heterojunction

The equivalent circuit of an organic PV cell is shown in Fig. 3, and forms for basis for our current model. The photocurrent source, J_{ph}, opposes the dark current, J_{dark}, which is limited by the series and parallel resistances, R_s and R_p, respectively. Here, $J(R_p)$ is the current flowing through R_p. The J-V characteristics of an organic PV cell can then be expressed by the generalized Shockley equation[15]

$$J = \frac{R_p}{R_s+R_p}\left\{J_S\left[\exp\left(\frac{q(V-JR_s)}{nk_BT}\right)-1\right]+\frac{V}{R_p}\right\} - J_{ph}(V) \quad (5)$$

where n is the diode ideality factor, and J_S is the reverse saturation current, *viz.*,[23]

$$J_S = J_{S0}\exp\left(-\frac{E_g}{2nk_BT}\right). \quad (6)$$

Here, E_g is the HJ activation energy barrier, equal to $E_g=IP_D-EA_A$, and J_{S0} is a temperature independent prefactor. The photocurrent density in Eq. (5) is

$$J_{ph}(V) = \int \frac{q\lambda}{hc}\eta_{EQE}(\lambda,V)S(\lambda)d\lambda, \quad (7)$$

where $S(\lambda)$ is the spectral irradiance of the incident light, and c is the speed of light. By inserting Eqs. (1) and (4) into Eq. (7),

$$J_{ph}(V) = P_0R_0H(V). \quad (8)$$

Here, $P_0=\int S(\lambda)d\lambda$ is the incident optical power density, and $R_0=\int\frac{q\lambda}{hc}\eta_A(\lambda)\,\eta_{ED}d\lambda$ is the responsivity for $\eta_{CT}=\eta_{CC}=1$, calculated using the transfer-matrix approach to determine the optical field intensity, and L_D in the D and A layers.[24]

The dark current density, J_{dark}, is also given by Eq. (5) when $J_{ph}=0$. From the $J-V$ characteristics, the short-circuit current density, J_{SC}, V_{OC}, the fill factor [FF $=\max(JV)/J_{SC}V_{OC}$], and the power conversion efficiency, $\eta_P=J_{SC}V_{OC}FF/P_0$, are calculated.

C. Maximum open-circuit voltage

To understand how V_{OC} changes with P_0 and T, we solve Eq. (5) at $J=0$ for $V=V_{OC}$,

TABLE I. Donor and acceptor materials and their corresponding ionization potentials (IP), electron affinities (EA), and optical energy gaps (E_{opt}).

Label[a]	Material[b]	IP[c] (eV)	EA (eV)[d]	E_{opt} (eV)	Reference
1	CuPc	5.2(7)	3.2(7)	1.7	43
2	Pentacene	5.1(9)	3	1.8(8)	43
3	NPD	5.5	1.7	3.1	43
4	SubPc	5.6		2.0	38
5	$Ru(acac)_3$	4.9		2.1	25
A	C_{60}	6.2(4)	3.6	1.8	44
B	C_{70}	6.4(1)	4.3	1.7(3)	44
C	PTCBI	6.2	3.6	1.7	43
D	PTCDA	6.8	4.6	2.2	43

[a]Numbers represent donor materials while letters represent acceptor materials.
[b]CuPc, copper phthalocyanine; NPD, *N*,*N*′-di-1-naphthyl-*N*,*N*′-diphenyl-1,1′-biphenyl-4,4′diamine; SubPc, boron subphthalocyaninechloride; $Ru(acac)_3$, ruthenium (III) trisacetylacetonato; PTCBI, 3,4,9,10-perylenetetracarboxylic bisbenzimidazole, and PTCDA, perylene-3,4,9,10-tetracarboxylic-3,4,9,10-dianhydride.
[c]Measured with ultraviolet photoemission spectroscopy with an error of ±0.1 eV.
[d]Measured with inverse photoemission spectroscopy with an error of ±0.5 eV.

$$V_{OC} = \frac{nk_BT}{q} \ln\left(\frac{J_{ph}(V_{OC})}{J_S} + 1 - \frac{V_{OC}}{J_S R_p}\right). \quad (9)$$

Equations (8) and (9) show that as P_0 increases, $V_{OC} \propto \ln(P_0)$ assuming that n and $H(V_{OC})$ are constant, and the product $J_S R_p \gg V_{OC}$. This is true at P_0 less than a few suns intensity (1 sun=100 mW/cm^2), but for larger P_0, $R_p \propto P_0^{-1}$ (see Sec. IV A) and $H(V_{OC})$ decreases. As P_0 is increased further, V_{OC} saturates at a maximum, V_{OC}^{max}. Similarly, as T is reduced, $V_{OC} \propto T^{-1}$ owing to the rapid reduction of $J_S(T)$ [see Eq. (6)]. Ultimately, however, as $H(V_{OC})$ decreases with T, V_{OC} again saturates at the same V_{OC}^{max} (see Sec. IV B).

Now, V_{OC}^{max} is achieved when the quasi-Fermi levels of the donor and acceptor layers become pinned at high currents. Examining the energy level diagram in Fig. 1, and taking into account exciton bonding, the *intrinsic* open circuit voltage, which corresponds to V_{OC}^{max}, can be written as

$$qV_{OC}^{max} = IP_D - EA_A - \frac{q^2}{4\pi\varepsilon_0\varepsilon_r r}, \quad (10)$$

where ε_0 is the vacuum permittivity, ε_r is the relative dielectric constant of the bulk organic material, and r_{DA} is the initial separation distance of the optically generated hole and electron pair in the donor and acceptor layers, respectively, immediately following charge transfer. The third term on the right-hand side of Eq. (10) corresponds to the binding energy, E_B, of the bound electron-hole geminate pair following charge transfer.

III. EXPERIMENT

Organic HJs were grown on glass substrates precoated with a 1500 Å thick, transparent conducting indium tin oxide (ITO) anode with a sheet resistance of 15 Ω/□. Prior to organic deposition, the substrates were cleaned in acetone, isopropanol, and trichloroethylene followed by exposure to UV ozone for 5 min. The organic films and a metal cathode were deposited via high vacuum thermal evaporation in a chamber with a base pressure of 2×10^{-7} Torr. The organic source materials were purified by three gradient sublimation cycles prior to use.[3] In all cases, the structure is ITO/donor/acceptor/exciton blocking layer (EBL)/cathode. The various donors and acceptors and their energy levels used in this work are listed in Table I. The values of IP were obtained from ultraviolet photoemission spectroscopy, whereas EA was taken from inverse photoemission spectroscopy measurements at the low energy edge of the LUMO signal. The donor (acceptor) layers were each at least 150 (250) Å thick. The exciton blocking layer (EBL) was composed of a 100 Å thick layer of bathocuproine (BCP).[25] A 1000 Å thick Ag, Al, or Au cathode was evaporated through a shadow mask with 0.8 mm^2 circular openings defining the device active area.

Current-voltage characteristics in the dark and under simulated air mass global (AM1.5G) solar illumination from a 1000 W Xe-arc lamp were measured using an HP 4155B semiconductor parameter analyzer. The samples were placed in an open cycle liquid He cryostat. Temperature was measured using a Si diode sensor placed on the sample surface. The illumination intensity was varied using neutral density filters, and measured with a calibrated Si detector coupled to a broadband optical power meter.

IV. RESULTS

A. Device current in the dark and under illumination

Figure 4(a) shows the dark *J*-*V* characteristics in 20 K steps over the temperature range 120 K$\leqslant T\leqslant$ 300 K for the structure: ITO/200 Å copper phthalocyanine (CuPc)/400 Å C_{60}/BCP/Al. The data are shown by open circles, while the lines are fits to the data using Eq. (5), with

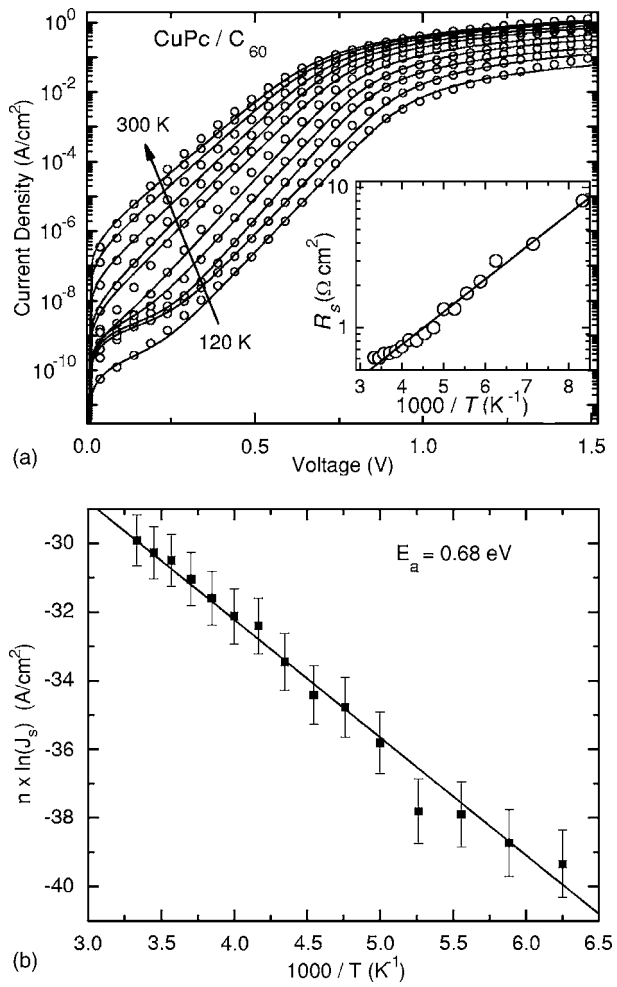

FIG. 4. (a) Dark current density versus voltage (J_{dark}-V) characteristics (open circles) over the temperature range 120 K$\leqslant T \leqslant$300 K at 20 K intervals for the heterojunction structure: ITO/CuPc(200 Å)/C_{60}(400 Å)/BCP(100 Å)/Al(1000 Å). The solid lines are fits to the J-V characteristics based on Eq. (5) in text. Inset: The specific series resistance, R_s vs T^{-1} for the same structure extracted from the fits. (b) The parameter $n\ln(J_S)$ (J_S the reverse saturation current density) vs T^{-1} for the device of (a). The solid line is a linear fit to $n\ln(J_S)$, satisfying Eq. (6) in text with an activation energy 0.68 eV.

$J_{\text{ph}}(V)=0$. The values of $n\ln(J_S)$ extracted from the data in Fig. 4(a) are shown in Fig. 4(b) versus $1000/T$. Over this temperature range, n decreases from $n=2$ at 300 K, to 1.6 at 150 K. The dependence of the specific series resistance, $R_s(T)$, is plotted in the inset of Fig. 4(a).

The J-V characteristics of the device in Fig. 4 in the dark (squares) and under AM1.5G illumination of 1.5 suns intensity (circles) are replotted on a linear current scale in Fig. 5. To simulate the device under illumination, we use Eq. (8) to define $J_{\text{ph}}(V)$, and let $R_p=R_p(P_0)$, to represent the light-intensity-dependent specific parallel resistance.[26,27] The fits are shown in Fig. 5, with both theory and experiment yielding $V_{\text{OC}}=(0.5\pm0.02)$ V and FF=0.58±0.01. The inset of Fig. 5 shows R_p versus P_0, where R_p decreases from $3\times10^5\ \Omega\ \text{cm}^2$ at 0.15 mW/cm^2, to $R_p=320\ \Omega\ \text{cm}^2$ at

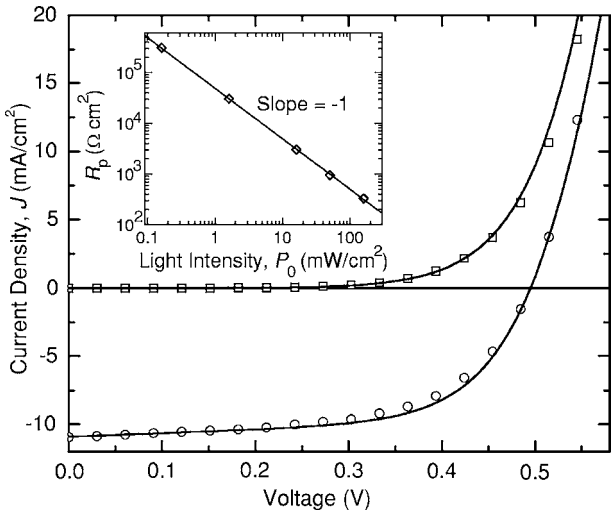

FIG. 5. Linear current density versus voltage (J-V) characteristics for the device of Fig. 4 at 300 K in the dark (open squares) and under an incident optical intensity (P_0) of 150 mW/cm^2 (open circles). The solid lines are fits to the data as described in the text. Inset: The specific parallel resistance under illumination, R_p versus P_0. The solid line is a linear best fit to the data.

150 mW/cm^2, following $R_p=(45\pm5\ \Omega\ \text{W})/P_0$ over more than three orders of magnitude in incident power.

B. Temperature dependence

Figures 6(a) and 6(b) show V_{OC} and FF, respectively, for the device in Figs. 4 and 5 as functions of T. Here, V_{OC} increases inversely with T until approximately 175 K, at which point V_{OC} saturates for a given P_0. The value of V_{OC} at a constant T also increases with P_0, consistent with Eq. (9). The FF of the device reaches a peak of 0.65 at 225 K, and decreases rapidly at $T<200$ K.

Figure 7 shows the dependence of V_{OC} on T under illumination for several DA pairs and cathode (Ag, Al, Au) combinations. For the CuPc/C_{60} structure in Fig. 3, V_{OC} saturates for both Al (open circles) and Au (filled squares) at approxi-

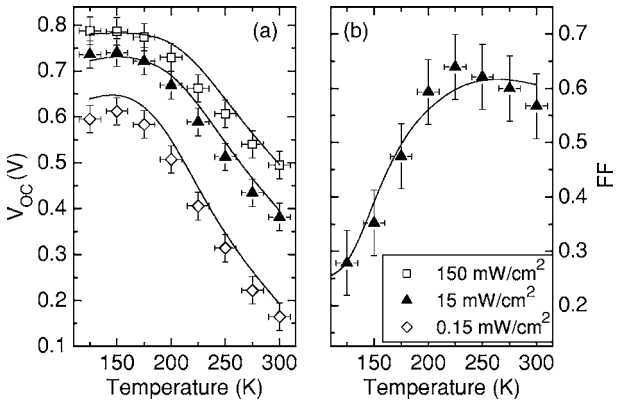

FIG. 6. Temperature dependencies of (a) the open-circuit voltage (V_{OC}) at various incident optical light intensities, and (b) fill factor (FF), for the CuPc/C_{60} heterostructure of Fig. 4. The solid lines are fits to the data as described in the text.

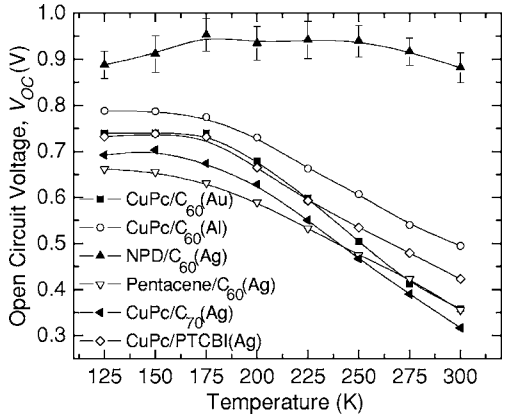

FIG. 7. Open-circuit voltage (V_{OC}) versus T for various donor-acceptor heterojunctions. The metal in parentheses in the legend indicates the cathode material for that device. The error bars displayed for the NPD/C_{60} (Ag) device are typical for all of the heterojunctions.

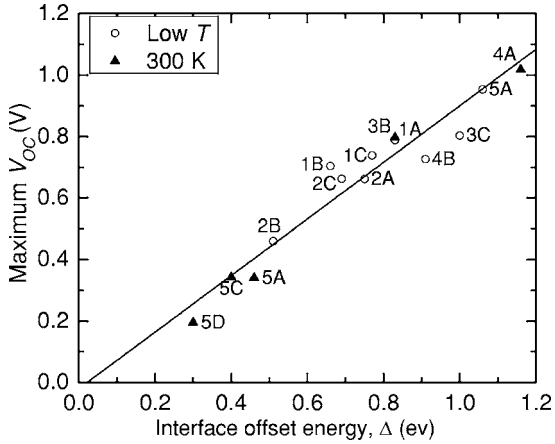

FIG. 8. The maximum value of the open-circuit voltage (V_{OC}^{max}) for different donor-acceptor photovoltaic cells versus the interface energy Δ as defined in text. The closed triangles correspond to heterojunction devices for which the maximum open circuit voltage, V_{OC}^{max}, was measured at 300 K, whereas open circles are V_{OC}^{max} collected at $T<300$ K. The solid line shows a linear best fit to the data (slope=0.92 and intercept=−0.02). The various letters and numbers for each point refer to materials listed in Table I.

mately 175 K, with $V_{OC}^{max}=(0.79\pm0.03)$ V for Al, and (0.76 ± 0.02) V for Au. In contrast, $V_{OC}(T)$ for the N,N'-di-1-naphthyl-N,N'-diphenyl-1,1′-biphenyl-4,4′ diamine (NPD)/C_{60} HJ is relatively temperature independent. This HJ reaches saturation at 300 K for $P_0>1$ sun, similar to previously reported polymer blend junctions.[28]

Figure 8 shows V_{OC}^{max} for 14 *DA* pairs plotted vs the interface offset energy, $\Delta=IP_D-EA_{opt,A}$ (see Fig. 1). Here, $EA_{opt,A}$ is the electron affinity of the acceptor as determined from its optical energy gap. Open circles correspond to V_{OC}^{max} taken at low T, whereas filled triangles represent V_{OC}^{max} at 300 K at high P_0. The labels for each point correspond to the molecules listed in Table I. The line corresponds to a linear best fit through the data with slope=(0.92 ± 0.02), and intercept=$-(0.02\pm0.03)$ V.

V. DISCUSSION

A. Heterojunction current

The J-V characteristic fit to the generalized Shockley theory [Eq. (5)] suggests that the heterojunction at the *DA* interface is well defined and planar. Also, $n=2$ at 300 K implies that the *DA* junction dark current is dominated by recombination. Further evidence is provided in Fig. 4(b), where the fit of $n\ln(J_S)$ to $1/T$ corresponding to Eq. (6) (solid line) indicates that this quantity is thermally activated with energy $E_g/2=(0.68\pm0.06)$ eV. This is consistent with the[23] CuPc/C_{60} HJ, where $E_g=IP_D-EA_A=(1.6\pm0.6)$ eV. The discrepancy of ~0.2 eV is due to errors associated with the inverse photoelectron spectroscopic measurement of EA_A (see Table I). Hence, the *DA* HJ is the dominant factor in determining the dark J-V characteristics. The value of J_S, in particular, affects V_{OC} [cf. Eq. (9)] and, in turn, FF, as described below. The other extracted dark current fit parameters (listed in Table II) reveal that R_p is not strongly temperature dependent, while the inset to Fig. 4(a) suggests that $R_s \propto \exp(-E_a/k_BT)$, with a small activation energy of $E_a=5$ meV, most likely due to an increase in the bulk hole and electron mobilities with decreasing T.

TABLE II. Parameters from Eq. (5) in text for various donor/acceptor heterojunction combinations at 300 K in the dark.

Donor-Acceptor interface[a]	J_S (A/cm^2)	n	R_s (Ω cm^2)	R_p (Ω cm^2)
Pentacene/C_{70}	3.3×10^{-5}	2.1	3.4	3.5×10^{4}
CuPc/C_{70}	1.0×10^{-5}	2.0	0.7	7.9×10^{4}
Pentacene/C_{60}	2.7×10^{-6}	2.0	0.1	8.1×10^{4}
Pentacene/PTCBI	2.5×10^{-7}	1.6	0.7	5.0×10^{5}
CuPc/C_{60}	1.0×10^{-6}	2.0	0.1	1.1×10^{6}
CuPc/PTCBI	5.5×10^{-7}	1.7	0.2	9.1×10^{5}
NPD/C_{60}	7.1×10^{-10}	2.6	28.4	2.2×10^{6}
SubPc/C_{60}	5.8×10^{-9}	1.6	0.9	1.2×10^{5}

[a]See Table I for chemical name.

TABLE III. Parameters for Eq. (3) in text for various donor-acceptor interfaces.

Donor-Acceptor interface[a]	Donor to Acceptor		Acceptor to Donor		
	k_{ccD} (s^{-1})	λ_{ccD} (eV)[b]	k_{vvA} (s^{-1})	λ_{vvA} (eV)[b]	λ_{cv} (eV)[b]
Pentacene/C_{60}	$(8\pm2)\times10^{11}$	0.9	$(3\pm1)\times10^{11}$	1.1	0.8
CuPc/C_{60}	$(2\pm0.7)\times10^{10}$	1.0	$(2\pm0.9)\times10^{11}$	0.6	0.7
CuPc/PTCBI	$(4\pm1)\times10^{8}$	0.8	$(1\pm0.8)\times10^{9}$	0.6	0.7
NPD/C_{60}	$(1\pm0.8)\times10^{7}$	1.3	$(4\pm1)\times10^{7}$	0.4	0.9
CuPc/C_{70}	$(2\pm0.9)\times10^{11}$	0.7	$(3\pm1)\times10^{11}$	0.7	0.7
Pentacene/C_{70}	$(4\pm1)\times10^{10}$	0.9	$(3\pm2)\times10^{11}$	0.7	0.5

[a]See Table I for chemical name.
[b]Fit parameter with an error of ±0.1 eV.

Resistance also plays a role in the fill factor,[15]

$$\mathrm{FF}(R_s,R_p)\approx \mathrm{FF}(0,\infty)\left(1-\frac{J_{\mathrm{SC}}R_s}{V_{\mathrm{OC}}}-\frac{V_{\mathrm{OC}}}{J_{\mathrm{SC}}R_p}\right). \quad (11)$$

Equation (11) indicates that FF is reduced below its maximum in junctions with high R_s and low R_p. The thermally activated R_s provides the dominant resistive contribution to the decrease in FF with T (see Fig. 6), although this is small in comparison with the FF dependence of $V_{\mathrm{OC}}(T)$.

In contrast, there is an inverse dependence of R_p on light intensity (Fig. 5, inset). This has also been reported for pentacene/C_{60} cells[26] as well as for bulk HJ polymer/fullerene devices.[27,29] This suggests that photoconductivity in the separate D and A layers contributes to free electron and hole generation, in addition to charge transfer at the DA heterointerface. Photoconductivity in homogeneous organic semiconductors has been widely observed, and is often attributed to exciton dissociation in the bulk of the D and A layers due to their interaction with trapped charges, impurities, defects, and other material imperfections.[30,31] For example, an exciton can undergo annihilation on collision with a trapped charge, resulting in free carrier emission to the LUMO. This process is expected to produce charge carriers with a linear dependence on exciton density, which in turn is linearly dependent on P_0, consistent with Fig. 5. The photoconductive quantum efficiency can be estimated using $\eta_{\mathrm{PC}}=L^2V_{\mathrm{ph}}/(R_pP_0\tau_{\mathrm{rec}}\mu)$, where $V_{\mathrm{ph}}\sim2$ eV is the photon voltage, $L=50$ nm is the D or A layer thickness, $\tau_{\mathrm{rec}}\sim5$ ns is the carrier recombination time, and $\mu\sim10^{-2}$ cm^2/V s is the charge mobility within its respective transport layer. The data in Fig. 5 suggest $\eta_{\mathrm{PC}}\approx2\%$ for the CuPc/C_{60} HJ (compared to ~50% due to exciton dissociation at the HJ itself). This process, and its reduction of R_p with increasing P_0 represents a property that is intrinsic to organic HJs, and ultimately reduces FF and η_P at high light intensities in PV cells.

B. Open-circuit voltage of donor-acceptor heterojunctions

To probe the origin of V_{OC}, we compare $V_{\mathrm{OC}}^{\max}$ for the set of DA HJ materials combinations in Table III. This is in contrast with previous studies that have sought to correlate V_{OC} with material energy levels, where V_{OC} was measured at $T=300$ K, and typically at $P_0=1$ sun.[9–14] As shown in Fig. 7, $V_{\mathrm{OC}}^{\max}$ for CuPc/C_{60} HJs with either Al or Au cathodes (with work functions of $\phi_{mc}=4.3$ eV and 5.1 eV, respectively) differ by only 0.03 V, which is within the experimental error. This suggests that it is the DA pair energy levels that determine $V_{\mathrm{OC}}^{\max}$, and not the cathode material work function.[32] We note that previous studies have often shown a weak dependence[10] of V_{OC} on ϕ_{mc}, possibly due to measuring V_{OC} below $V_{\mathrm{OC}}^{\max}$.

Charge transfer at a DA interface results in a Coulombically bound electron-hole pair.[33] An estimate of the pair binding energy immediately following a nearest-neighbor charge transfer reaction gives $E_B\sim0.5$ eV$\gg k_BT$, assuming $\varepsilon_r=3$ and $r_{DA}=10$ Å [cf. Eq. (10)]. This is approximately equal to E_B for many small-molecular weight organic semiconductors.[20,21] Hence, in Fig. 8 we plot $V_{\mathrm{OC}}^{\max}$ vs $\Delta=\mathrm{IP}_D-\mathrm{EA}_{\mathrm{opt},A}$, where the best fit line to the data is consistent with a unity slope and an intercept at the origin. From this linear relationship, we conclude that the geminate polaron-pair[33,34] or exciplex[35,36] state is rapidly dissociated into free charge carriers, thereby contributing to the photocurrent. To fully dissociate, the exciplex must overcome the Coulombic attraction between the hole on a donor molecule and electron on a neighboring, interfacial acceptor molecule. Consequently, the largest potential developed across the HJ, $V_{\mathrm{OC}}^{\max}$, must account for this energy loss as expressed in Eq. (10).

We note that the relationship, $\Delta=\mathrm{IP}_D-EA_{\mathrm{opt},A}$, is only approximate. According to Fig. 1, the interface gap is equal to $\Delta=\mathrm{IP}_D-\mathrm{IP}_A+E_{\mathrm{opt},A}+E_{B,A}$, while the total energy that results from exciton dissociation should be simply $\mathrm{IP}_D-\mathrm{EA}_A$. However, on relaxation following charge transfer, the hole polarization results in a loss of $E_{B,D}/2$ and likewise, the electron loses $E_{B,A}/2$ as it relaxes from the LUMO. For most of the high mobility donors and acceptors considered here, the polarization energies for both holes and electrons in the D and A layers, respectively, are approximately equal. In this case, the resulting energy of the geminate pair is therefore approximately equal to $\Delta\cong\mathrm{IP}_D-\mathrm{EA}_A-E_B$, as expressed by Eq. (10) and in Fig. 1, and as observed. Note that the precise distribution of the energy loss between electron and hole is unimportant, as it is the total energy loss that determines the ultimate value of $V_{\mathrm{OC}}^{\max}$.

Note that $V_{\mathrm{OC}}^{\max}$ is not attainable for all DA HJs under standard operating conditions of $T=300$ K and $P_0=1$ sun

intensity, due to large values of J_S. Nevertheless, V_{OC}^{max} is obtained under normal operating conditions for NPD/C_{60} and boron subphthalocyaninechloride (SubPc)/C_{60} HJs.[37,38] The maximum potential difference observed for these two HJs is $V_{OC} \approx 1$ V, in contrast to, for example, the CuPc/C_{60} HJ, where $V_{OC} \approx 0.5$ V at 300 K and 1 sun versus $V_{OC}^{max} \approx 0.8$ V.

C. Electron transfer rate

As V_{OC} increases, the potential drop at the HJ decreases, thereby resulting in a concomitant decrease in J_{SC}. Hence, the maximum power conversion efficiency, $\eta_P = J_{SC} V_{OC} FF / P_0$, is obtained for the optimal combination of V_{OC} and J_{SC}. To estimate the effect of V_{OC} on J_{SC}, we must first determine the charge transfer rate at the HJ for a given *DA* pair. We begin by fitting $J_{ph}(V)$ characteristics of the *DA* HJ using nonadiabatic Marcus theory. This model describes intermolecular charge transfer at the *DA* interface, and the probability for separation of the geminate state immediately following this process. Once fully separated, the electrons and holes are collected at their respective contacts following transport through the homogeneous *A* and *D* layers.

The solid lines in Fig. 6 correspond to calculations based on Eqs. (5)–(9). The dark current is described by J_S, R_s, R_p, and n for each HJ pair (see Table II). To fit the photocurrent characteristics, J_S, R_s, and n determined in the dark are kept constant with P_0, and R_p and n independent of T. Also, J_S and R_s vary with T as discussed above. Parameters V_{if}, λ_{ccD}, λ_{vvA}, λ_{cv} are then used to fit the *J-V* characteristics vs P_0 and T. Here, V_{if} and λ_{cv} are assumed to be identical for both donor-to-acceptor ($D \rightarrow A$) and $A \rightarrow D$ transitions. The fitting procedure is repeated for each P_0 to obtain an average final value and error (shown in Fig. 9) for the electron transfer rate, k_{ET}.

Figure 9 is a plot of k_{ET} for $D \rightarrow A$ and $A \rightarrow D$ transfer for several *DA* HJs in Table I as a function of ΔE_{LUMO} and ΔE_{HOMO}, respectively. Here, k_{ET} increases with offset energy, eventually reaching a plateau, and then decreases once again at high energies, corresponding to highly exothermic electron transfer reactions. The region of energy that corresponds to increasing k_{ET} is the "normal" region, and decreasing k_{ET} occurs in the Marcus "inverted" region.[17] This behavior has previously been observed for electron transfer reactions in fullerenes.[39]

The $D \rightarrow A$ transition of the CuPc/C_{60} HJ yields $k_{ET} = (2.0 \pm 0.7) \times 10^{10}$ s^{-1}, comparable to $k_{ET} = 8 \times 10^{10}$ s^{-1} reported for a oligo(*p*-phenylene vinylene) fullerene dyad.[40] Furthermore, the various rates for the CuPc/C_{60} *DA* interface suggest that $H(0\ V) \approx 0.9$; i.e., 90% of excitons that reach a *DA* interface contribute to photocurrent. This is consistent with the high values of η_{EQE} that have been reported for the CuPc/C_{60} HJ.[41] The other HJs have $H(0\ V)$ varying from 0.6 to 0.95. This is comparable to the prediction of Mihailetchi *et al.*,[42] where a model based upon Onsager's theory of geminate recombination suggests $H(0\ V) = 0.6$ for a polymer-fullerene bulk heterojunction device. Now, k_{ET} decreases with T [cf. Eq. (9)], resulting in a similar reduction in both H(V) and J_{SC}. Indeed, J_{SC} exponentially decreases with T, similar to the behavior for polymer-fullerene bulk HJ devices,[27] and consistent with the model.

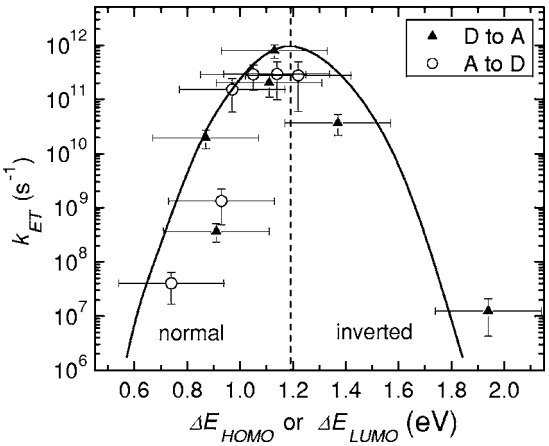

FIG. 9. The electron transfer rate, k_{ET}, for donor-to-acceptor transfer ($D \rightarrow A$, filled triangles) and acceptor-to-donor transfer ($A \rightarrow D$, open circles), versus the difference between the lowest unoccupied molecular orbitals (ΔE_{LUMO}) in the case of $D \rightarrow A$, and the difference between highest occupied molecular orbitals (ΔE_{HOMO}) in the case of $A \rightarrow D$. The line serves as a guide to the eye. The vertical dashed line delineates the so-called Marcus normal and inverted regions for charge transfer.

D. Efficiency limits to organic DA heterojunction cells

These findings have important consequences in the design of *DA* junctions used in organic PV cells. From the energy diagram of Fig. 1, a high V_{OC} is obtained by increasing Δ, since that results in a reduced J_S. To simulate an optimized structure that maximizes the product, $V_{OC} \cdot J_{SC}$, we used a genetic algorithm for a double heterostructure device with the following structure: ITO/*D*/*A*/EBL/Ag. The real part of the index of refraction is assumed to be 1.9 for both the *D* and *A* layers, and 1.7 for the EBL—values close to those of materials used in conventional cells.[22] The imaginary part of the index of refraction is taken equal to 1 for incident photon energies larger than the optical gap of the *D* and *A* layers, while it is 0 for the EBL. The diffusion length for both *D* and *A* is $L_D = 20$ nm. The algorithm then optimizes the thicknesses of the organic layers using a transfer-matrix approach that includes optical interference effects.[24]

We select $E_{opt,A} = 1.8$ eV, similar to that of C_{60}, as shown in the inset of Fig. 10(a). For the simulations at 1 sun AM1.5G solar illumination and $T = 300$ K, we use R_s, R_p, n, E_B, k_{ET}, and λ typical of archetype CuPc/C_{60} junctions given in Tables I and II. The results are shown in Fig. 10 for J_{SC} [Fig. 10(a)] with a maximum at $E_{opt,D} = 1.4$ eV. This is expected since a smaller optical gap material can harvest a larger percentage of the solar spectrum that extends well into the infrared. However, as the offset energy is increased to >1 eV, J_{SC} drops rapidly due to a decreasing ΔE_{LUMO} and ΔE_{HOMO}, which inhibit efficient exciton dissociation. The FF remains approximately constant at 0.7, since it is primarily controlled by both series and parallel resistance [cf. Eq. (11)].

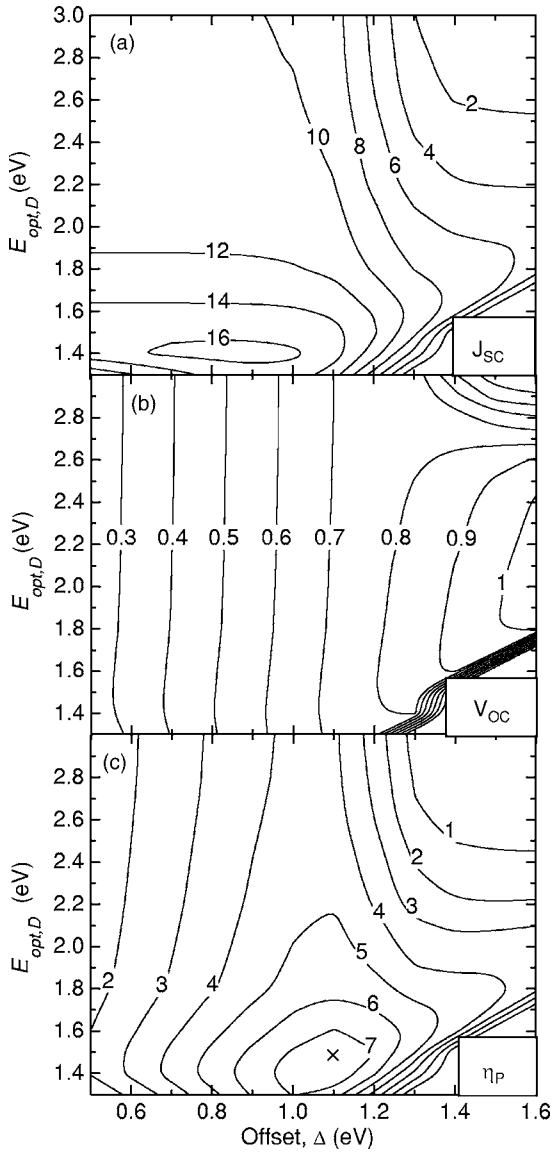

FIG. 10. Calculated contour plots of (a) short-circuit current density (J_{SC}[mA/cm^2]), (b) open-circuit voltage (V_{OC} [V]), and (c) power conversion efficiency (η_P [%]) for optimized device structures as functions of the donor (D) optical gap ($E_{\mathrm{opt},D}$) and offset energy, $\Delta = \mathrm{IP}_D - \mathrm{EA}_{\mathrm{opt},A}$ (see Fig. 1), where IP is the ionization potential, EA is the electron affinity, A is the acceptor material, and $\mathrm{EA}_{\mathrm{opt},A} = E_{\mathrm{opt},A} - \mathrm{IP}_A = 1.8$ eV. The general device structure is ITO/D/A/exciton blocking layer/Ag. The "×" in (c) shows the location of the maximum η_P.

Now, V_{OC} [Fig. 10(b)] increases monotonically with offset energy, with an approximately 0.3 V difference between V_{OC} and the offset, Δ. This difference arises from the operating conditions of $P_0 = 1$ sun and $T = 300$ K corresponding to $V_{OC} < V_{OC}^{\max}$, and is close to that reported for polymer-fullerene bulk HJs.[9] These device parameters result in a maximum $\eta_P = 7.9\%$ [corresponding to point "×" in Fig. 10(c)] for an optimized double heterostructure device, with $E_{\mathrm{opt},D} = 1.5$ eV and $\Delta = 1.1$ eV.

Using the optimized values of $E_{\mathrm{opt},A} = 1.8$ eV, $E_{\mathrm{opt},D} = 1.5$ eV, and $\Delta = 1.1$ eV, we next simultaneously vary the diffusion lengths, L_D, in the D and A layers. Figure 11 shows

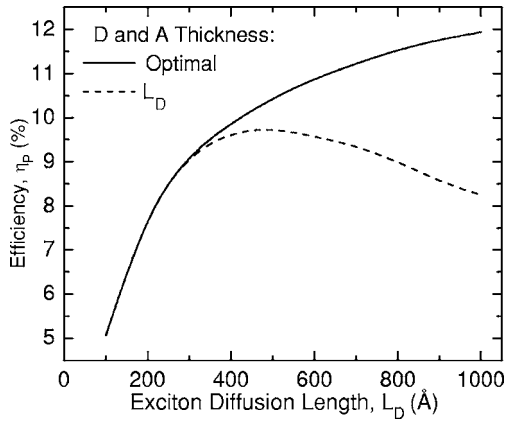

FIG. 11. Calculated power conversion efficiency (η_P) as a function of donor (A) and acceptor (A) exciton diffusion length, L_D, for the device structure: ITO/D/A/exciton blocking layer (EBL)/Ag as defined in text. The solid line shows the case of optimal D, A, and EBL layer thickness, while the dashed line shows the case where D and A thickness equals L_D.

the results of this simulation, where η_P increases monotonically until $L_D \approx 400$ Å. For $L_D \geq 400$ Å, η_P decreases due to a saturation of η_A, resulting in decreased absorption in the acceptor layer (dashed line). By choosing optimized D and A thicknesses (solid line), this decrease can be avoided, leading to $\eta_P \approx 12\%$ for $L_D = 1000$ Å. To further increase efficiency, a DA mixed layer can be inserted between the D and A layers[19] to achieve an approximately 25% increase in J_{SC}, yielding $\eta_P \approx 15\%$. Also, by stacking two such devices in a tandem geometry using materials that span a broader range of the solar spectrum than the CuPc/C_{60} system,[7] the efficiency can be increased to $\eta_P > 16\%$.

VI. CONCLUSIONS

We have presented a comprehensive device model that clarifies the interrelationships between the energetic characteristics of the donor and acceptor materials that comprise an organic heterojunction, and the limitations those characteristics impose when such a junction is employed in a photovoltaic cell. The model is based on the generalized Shockley equation for p-n junctions that describes the dark current characteristics of organic heterostructure barriers. The voltage dependent photocurrent is understood in the context of the Marcus theory of electron transfer, providing basic insights into the factors that govern the magnitude of the energy level offset between two contacting organic semiconductor materials. The electron transfer rates are shown to follow the predictions of Marcus theory, increasing with HOMO-HOMO and LUMO-LUMO offsets until reaching the inverted region, after which the rate decreases. Also, the HJ parallel resistance is found to be a linearly decreasing function of illumination intensity due to photoconductive charge generation. This effect may ultimately limit device efficiency.

The maximum open-circuit voltage for each donor-acceptor pair was measured, and was found to be a function of the difference between the donor ionization potential, ac-

ceptor electron affinity, and the exciplex binding energy. Based upon the fundamental understanding of the factors governing the offset energies at organic heterointerfaces in the absence of a high density of background charge, we find that power conversion efficiencies approaching 12% are possible for a single HJ cell, increasing to more than 16% by incorporating tandem solar cell structures. Ultimately, our models of charge transfer at organic heterointerfaces suggests that there exists an intrinsic compromise between increasing J_{SC} by tuning the HOMO-HOMO and LUMO-LUMO offsets and optical gaps, and increasing V_{OC} by increasing the difference between the donor HOMO and acceptor LUMO. This compromise forms the ultimate limitation to the power conversion efficiency obtainable by an organic *DA* HJ cell structure.

ACKNOWLEDGMENTS

The authors gratefully acknowledge the National Renewable Energy Laboratory, the Air Force Office of Scientific Research, and Global Photonic Energy Corporation for partial support of this work.

APPENDIX

To determine the donor current density vs voltage characteristic, J_D vs V, G_{vcD} is found following Ref. 16. That is

$$G_{vcD} = q\left(\phi_s + \phi_a - \frac{k_g}{x_c^2 - 1}\right)\left(\frac{x_c - 1}{x_c + 1}\right), \tag{A1}$$

where $x_c = 1/f_c - 1$, k_g is the recombination rate given as $k_g = f_{\text{osc}}(2\pi E_{\text{opt}}^2/h^3c^2)$, and ϕ_s and ϕ_a are the solar and ambient spectral photon flux densities, respectively. Thus[16]

$$\phi_s = \frac{2\pi F_s f_{\text{osc}}}{c^2 h^3} \frac{E_{\text{opt}}^2}{\exp(E_{\text{opt}}/k_B T_s) - 1} \tag{A2}$$

and

$$\phi_a = \frac{2\pi(1 - F_s) f_{\text{osc}}}{c^2 h^3} \frac{E_{\text{opt}}^2}{\exp(E_{\text{opt}}/k_B T) - 1}. \tag{A3}$$

The oscillator strength, $f_{\text{osc}} = 1 \times 10^{-21}$ eV m^2, $F_s = 2.16 \times 10^{-5}$ is the relative angular range of the sun, and $T_s = 5760$ K is the black-body temperature of the sun.

Now,

$$qV = 2(\text{IP}_D - \text{EA}_A) - E_{\text{tran},D} - 2k_B T \ln x_a - k_B T \ln x_c, \tag{A4}$$

where $x_a = 1/f_a - 1$, and

$$f_a = \frac{k_{ccD} - k_{cvD}\delta_{cvD}(1 - f_c) - G_{vcD}/q}{(k_{ccD} - k_{cvD})f_c + (k_{ccD}\delta_{ccD} - k_{cvD}\delta_{cvD})(1 - f_c)}, \tag{A5}$$

where $\delta_{if} = \exp[-(E_i - E_f)/k_B T]$. The limits on x_c are found by solving the quadratic equations that result from setting the probability, f_a, equal to 0 and 1. Then, from a known set of x_c, J_{ccD}, and J_{cvD}, then J_D, and V are calculated. The same procedure also is also used to find the acceptor J_A-V. This model for charge transfer using nonadiabatic Marcus theory differs from that described previously[16] in that it is applicable to both symmetric and asymmetric donor-acceptor heterojunctions.

*Electronic address: stevefor@umich.edu

[1] S. M. Sze, *Physics of Semiconductor Devices*, 2nd ed. (Wiley, New York, 1981).
[2] I. G. Hill, D. Milliron, J. Schwartz, and A. Kahn, Appl. Surf. Sci. **166**, 354 (2000).
[3] S. R. Forrest, Chem. Rev. (Washington, D.C.) **97**, 1793 (1997).
[4] S. R. Forrest, MRS Bull. **30**, 28 (2005).
[5] G. Dennler and N. S. Sariciftci, Proc. IEEE **93**, 1429 (2005).
[6] S. E. Gledhill, B. Scott, and B. A. Gregg, J. Mater. Res. **20**, 3167 (2005).
[7] J. Xue, S. Uchida, B. P. Rand, and S. R. Forrest, Appl. Phys. Lett. **85**, 5757 (2004).
[8] G. Li, V. Shrotriya, J. S. Huang, Y. Yao, T. Moriarty, K. Emery, and Y. Yang, Nat. Mater. **4**, 864 (2005).
[9] M. C. Scharber, D. Wuhlbacher, M. Koppe, P. Denk, C. Waldauf, A. J. Heeger, and C. J. Brabec, Adv. Mater. (Weinheim, Ger.) **18**, 789 (2006).
[10] C. J. Brabec, A. Cravino, D. Meissner, N. S. Sariciftci, T. Fromherz, M. T. Rispens, L. Sanchez, and J. C. Hummelen, Adv. Funct. Mater. **11**, 374 (2001).
[11] C. J. Brabec, A. Cravino, D. Meissner, N. S. Sariciftci, M. T. Rispens, L. Sanchez, J. C. Hummelen, and T. Fromherz, Thin Solid Films **403**, 368 (2002).
[12] X. Y. Deng, L. P. Zheng, C. H. Yang, Y. F. Li, G. Yu, and Y. Cao, J. Phys. Chem. B **108**, 3451 (2004).
[13] A. Gadisa, M. Svensson, M. R. Andersson, and O. Inganas, Appl. Phys. Lett. **84**, 1609 (2004).
[14] T. Kietzke, D. A. M. Egbe, H. H. Horhold, and D. Neher, Macromolecules **39**, 4018 (2006).
[15] R. H. Bube and A. L. Fahrenbruch, *Advances in Electronics and Electron Physics* (Academic, New York, 1981), p. 163.
[16] J. Nelson, J. Kirkpatrick, and P. Ravirajan, Phys. Rev. B **69**, 035337 (2004).
[17] R. A. Marcus and N. Sutin, Biochim. Biophys. Acta **811**, 265 (1985).
[18] B. P. Rand, P. Peumans, and S. R. Forrest, J. Appl. Phys. **96**, 7519 (2004).
[19] J. Xue, B. P. Rand, S. Uchida, and S. R. Forrest, Adv. Mater. (Weinheim, Ger.) **17**, 66 (2005).
[20] M. Knupfer, Appl. Phys. A: Mater. Sci. Process. **77**, 623 (2003).
[21] I. G. Hill, A. Kahn, Z. G. Soos, and R. A. Pascal, Chem. Phys. Lett. **327**, 181 (2000).
[22] P. Peumans, A. Yakimov, and S. R. Forrest, J. Appl. Phys. **93**, 3693 (2003).
[23] A. L. Fahrenbruch and J. Aranovich, *Solar Energy Conversion* (Springer-Verlag, New York, 1979), p. 257.

[24] L. A. A. Pettersson, L. S. Roman, and O. Inganas, J. Appl. Phys. **86**, 487 (1999).
[25] B. P. Rand, J. Li, J. Xue, R. J. Holmes, M. E. Thompson, and S. R. Forrest, Adv. Mater. (Weinheim, Ger.) **17**, 2714 (2005).
[26] S. Yoo, B. Domercq, and B. Kippelen, J. Appl. Phys. **97**, 103706 (2005).
[27] I. Riedel, J. Parisi, V. Dyakonov, L. Lutsen, D. Vanderzande, and J. C. Hummelen, Adv. Funct. Mater. **14**, 38 (2004).
[28] J. A. Barker, C. M. Ramsdale, and N. C. Greenham, Phys. Rev. B **67**, 075205 (2003).
[29] C. Waldauf, M. C. Scharber, P. Schilinsky, J. A. Hauch, and C. J. Brabec, J. Appl. Phys. **99**, 104503 (2006).
[30] M. Pope and C. E. Swenberg, *Electronic Processes in Organic Crystals and Polymers*, 2nd ed. (Oxford University Press, New York, 1999).
[31] J. Reynaert, V. I. Arkhipov, P. Heremans, and J. Poortmans, Adv. Funct. Mater. **16**, 784 (2006).
[32] B. A. Gregg and M. C. Hanna, J. Appl. Phys. **93**, 3605 (2003).
[33] T. Offermans, S. C. J. Meskers, and R. A. J. Janssen, Chem. Phys. **308**, 125 (2005).
[34] P. Peumans and S. R. Forrest, Chem. Phys. Lett. **398**, 27 (2004).
[35] A. C. Morteani, P. Sreearunothai, L. M. Herz, R. H. Friend, and C. Silva, Phys. Rev. Lett. **92**, 247402 (2004).
[36] T. Offermans, P. A. van Hal, S. C. J. Meskers, M. M. Koetse, and R. A. J. Janssen, Phys. Rev. B **72**, 045213 (2005).
[37] G. P. Kushto, W. H. Kim, and Z. H. Kafafi, Appl. Phys. Lett. **86**, 093502 (2005).
[38] K. L. Mutolo, E. I. Mayo, B. P. Rand, S. R. Forrest, and M. E. Thompson, J. Am. Chem. Soc. **128**, 8108 (2006).
[39] S. Fukuzumi, K. Ohkubo, H. Imahori, and D. M. Guldi, Chem.-Eur. J. **9**, 1585 (2003).
[40] P. A. van Hal, R. A. J. Janssen, G. Lanzani, G. Cerullo, M. Zavelani-Rossi, and S. De Silvestri, Phys. Rev. B **64**, 075206 (2001).
[41] J. Xue, B. P. Rand, S. Uchida, and S. R. Forrest, J. Appl. Phys. **98**, 124903 (2005).
[42] V. D. Mihailetchi, L. J. A. Koster, J. C. Hummelen, and P. W. M. Blom, Phys. Rev. Lett. **93**, 216601 (2004).
[43] A. Kahn, N. Koch, and W. Y. Gao, J. Polym. Sci., Part B: Polym. Phys. **41**, 2529 (2003).
[44] P. J. Benning, D. M. Poirier, T. R. Ohno, Y. Chen, M. B. Jost, F. Stepniak, G. H. Kroll, J. H. Weaver, J. Fure, and R. E. Smalley, Phys. Rev. B **45**, 6899 (1992).